Weak Localization in Graphene Flakes

F. V. Tikhonenko, D. W. Horsell, R. V. Gorbachev, and A. K. Savchenko
School of Physics, University of Exeter, Stocker Road, Exeter, EX4 4QL, United Kingdom
(Received 14 August 2007; published 6 February 2008)

We show that the manifestation of quantum interference in graphene is very different from that in conventional two-dimensional systems. Because of the chiral nature of charge carriers, it is not only sensitive to inelastic, phase-breaking scattering, but also to a number of elastic scattering processes. We study weak localization in different samples and at different carrier densities, including the Dirac region, and find the characteristic rates that determine it. We show how the shape and quality of graphene flakes affect the values of the elastic and inelastic rates and discuss their physical origin.

DOI: 10.1103/PhysRevLett.100.056802 PACS numbers: 73.23.−b, 72.15.Rn, 73.43.Qt

The quantum correction to the conductivity of two-dimensional systems due to electron interference has been studied for more than 20 years [1,2]. This phenomenon of weak localization (WL) has become a tool to determine the processes responsible for electron dephasing due to inelastic electron scattering or scattering by magnetic impurities [2,3]. In this well-established field of research it comes as a surprise to discover that in a new two-dimensional system, graphene [4], WL does not follow the standard convention that it is only controlled by inelastic and spin-flip processes. First attempts to measure WL in graphene have produced contradictory results that tentatively point towards this unusual behavior [5–7]. Measurements on graphene flakes fabricated by mechanical exfoliation [5] have shown that in the majority of samples WL is totally suppressed. In contrast, in a sample fabricated by an alternative, epitaxial method, WL has been distinctly seen, albeit at a single (high) carrier density [7].

The theory of WL in graphene [8] predicts a remarkable feature: it should be sensitive not only to inelastic, phase-breaking processes, but also to different *elastic* scattering mechanisms [8–10]. The reason for this is that charge carriers in graphene are *chiral*, that is, they have an additional quantum number (pseudospin) [11]. Elastic scattering that breaks the chirality will destroy the interference within each of the two graphene valleys in k space. Such defects, characterized by the scattering rate τ_s^{-1}, include surface ripples, dislocations and atomically sharp defects [5,10]. Intravalley WL can also be destroyed by anisotropy of the Fermi surface in k space, so called "trigonal warping" [8], characterized by the rate τ_w^{-1}. There is one elastic process, however, which acts to restore the suppressed interference. This is *intervalley* scattering, which occurs at a rate τ_i^{-1} on defects with size of the order of the lattice spacing a. As the two valleys have opposite chirality and warping, intervalley scattering is expected to negate the chirality breaking and warping effects by allowing interference of carriers from different valleys.

In this work we aim to examine what factors are responsible for the manifestation of WL in graphene fabricated by mechanical exfoliation [4]. We study the magnetoconductivity (MC) in perpendicular fields of several samples with different quality and dimensions, with the aim to control the relation between the scattering rates of carriers. These studies are performed at different carrier densities controlled by a gate voltage V_g, which include densities around the Dirac point at $V_g = 0$. This point is special as about it there is a change of the type of carrier from electrons to holes and therefore the net carrier density is zero. The conductivity, however, is seen to remain at a finite value and not drop to zero [12].

Figure 1 shows the resistivity as a function of V_g of four samples with different shapes and mobilities: D, F1, F2,

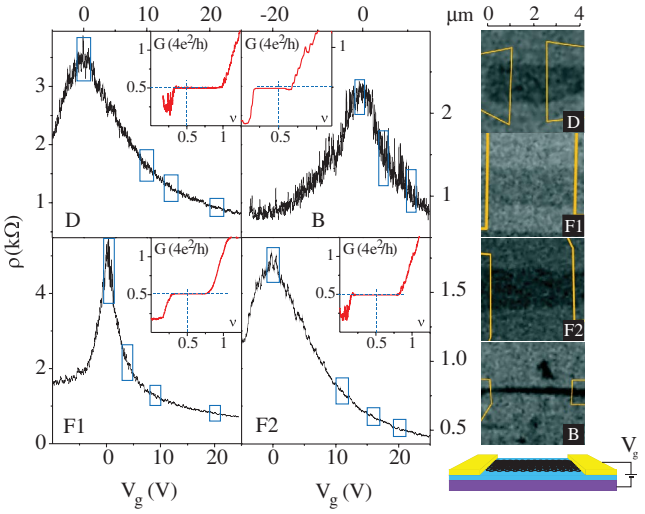

FIG. 1 (color). Resistivity of graphene flakes as a function of V_g at $T = 0.25$ K. The mobilities (in $\mathrm{cm^2\,V^{-1}\,s^{-1}}$) of the samples outside the Dirac region: 5100 (D), 7500 (F1), 10 000 (F2), and 8000 (B). The insets show the first quantum Hall plateau, where filling factor $\nu = nh/4eB$. The right panel shows scanning electron micrograph images of the samples, where the positions of the contacts are shown as outlines. The diagram at the foot of this panel shows the graphene sample on n^+Si substrate (purple), covered by 300 nm SiO_2 (blue) and contacted by Au/Cr (yellow). Control of the carrier density n is achieved by V_g.

and B, each with a typical peak around the Dirac point. Sample D is a square flake; F1 and F2 are rectangular with similar width to, but length larger than D; B is a narrow strip of similar length to F1 and F2 but with much smaller width, Fig. 1 (right). Insets in Fig. 1 demonstrate measurements of the first quantum Hall plateau, which shows a half-integer step $(0.5 \times 4e^2/h)$—a clear indication that the samples are single-layer graphene [12]. We wanted to see what difference the shape of the samples will make to the WL—e.g., the narrowest sample B is expected to have the largest scattering rate τ_i^{-1}, as the edges could produce strong intervalley scattering. To understand the relation between the scattering and the details of the graphene surface, the electrical measurements have been complemented by atomic force microscope (AFM) imaging of the sample topography, which have shown the presence of ripples, and additional rapid folds (ridges) across sample B [13].

In order to study the conductivity correction caused by WL we must first account for the reproducible conductance fluctuations clearly seen in Fig. 1. They are also present as a function of magnetic field B and are caused by the fact that the graphene flakes are small (comparable to the dephasing length L_ϕ), so that the average effect of WL is of the same order as the fluctuations which have the same, quantum interference origin [2]. We use the procedure developed in [14] in the study of WL in bilayer graphene: $R(V_g)$ is measured at different B and the results are averaged over a range $\Delta V_g = 2$ V shown in Fig. 1 by boxes which contain a large number of fluctuations [13]. Examples of the obtained average MC, $\triangle\sigma(B) = \langle\sigma(V_g, B) - \sigma(V_g, 0)\rangle_{\Delta V_g}$, are shown in Fig. 2 for different samples. For the analysis of the results we use the theory [8] which predicts that the MC is controlled by several scattering rates, both inelastic (τ_ϕ^{-1}) and elastic $(\tau_i^{-1}, \tau_s^{-1}, \tau_w^{-1})$:

$$\frac{\pi h}{e^2} \cdot \Delta\sigma(B) = F\left(\frac{\tau_B^{-1}}{\tau_\phi^{-1}}\right) - F\left(\frac{\tau_B^{-1}}{\tau_\phi^{-1} + 2\tau_i^{-1}}\right) - 2F\left(\frac{\tau_B^{-1}}{\tau_\phi^{-1} + \tau_i^{-1} + \tau_*^{-1}}\right). \quad (1)$$

Here $F(z) = \ln z + \psi(0.5 + z^{-1})$, $\psi(x)$ is the digamma function, $\tau_B^{-1} = 4eDB/\hbar$, τ_ϕ^{-1} is the phase-breaking rate and $\tau_*^{-1} = \tau_s^{-1} + \tau_w^{-1}$. (The theory assumes that the momentum relaxation rate τ_p^{-1} is the highest in the system and comes from the Coulomb charges in the SiO_2 substrate and not atomically sharp defects, so that it does not affect the carrier chirality.) The first term in Eq. (1) is responsible for weak localization, while the terms with negative sign can result in "antilocalization."

We have found that among the different possible relations between the scattering rates, the following holds in all studied samples: the intravalley WL is strongly suppressed due to a large rate τ_*^{-1}, which approaches τ_p^{-1}; however, WL is clearly seen in all regions of the carrier density, due to significant intravalley scattering, $\tau_i^{-1} \sim \tau_\phi^{-1}$. At the same time, the shape of the MC curves can be very different as it is controlled by the interplay between all scattering rates involved, Fig. 2. Comparing two regions of carrier densities for square sample D [Dirac region (a) and electron region (b)] one can see that in (a) the curves have a much stronger downturn, indicating greater importance of the third (antilocalizing) term in Eq. (1) due to smaller rate τ_*^{-1}. For two geometrically similar samples F1 and F2 in Fig. 2(c), it is seen that sample F2 (with largest mobility) has a more rapid increase of the conductivity in smaller field (due to smaller τ_ϕ^{-1}) and more rapid downward turn of the curves at larger fields (due to smaller τ_i^{-1}). For the narrow sample B, Fig. 2(d), the MC curves do not turn down at all, indicating a very fast intervalley rate τ_i^{-1} and therefore unimportance of all terms in Eq. (1) apart from the first.

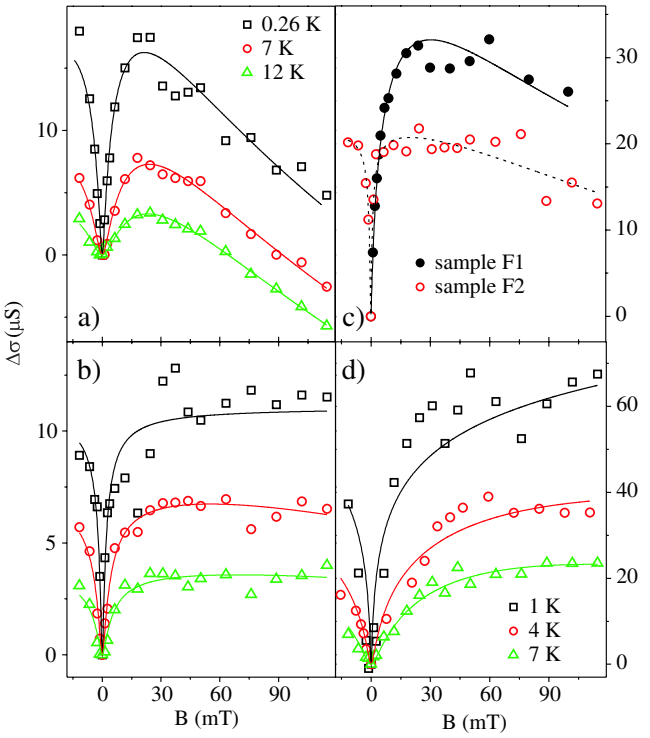

FIG. 2 (color online). Magnetoconductivity observed in graphene flakes. (a) Dirac region of sample D, $|V_g| \lesssim 1$ V, $n \lesssim 7 \times 10^{10}$ cm^{-2}; (b) sample D, $V_g \simeq 14$ V, $n \simeq 10^{12}$ cm^{-2} (the legends of (a) and (b) are the same); (c) samples F1 and F2 at $T = 1$ K, $V_g \simeq 10$ V, $n \simeq 7 \times 10^{11}$ cm^{-2}; (d) sample B, $V_g \simeq 11$ V, $n \simeq 8 \times 10^{11}$ cm^{-2}. Lines are best fits to Eq. (1).

Figure 3 shows the temperature dependence of the characteristic lengths found from the analysis of the MC by the best fit with Eq. (1). Figures 3(a) and 3(b) compare the results for the Dirac and electron regions for sample D, where it is seen that L_ϕ is temperature dependent at high T (≥ 3 K) but saturates at a value L_ϕ^{sat} at low temperatures. Figures 3(b) and 3(d) compare the results for samples D and F2 at close values of carrier densities outside the Dirac

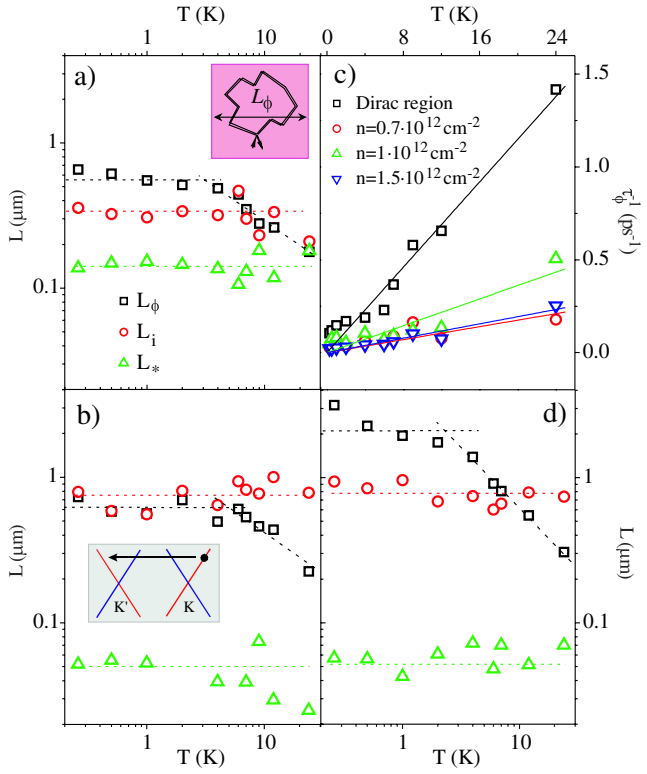

FIG. 3 (color online). Characteristic lengths responsible for weak localization; dotted lines are guides to the eye. Sample D: (a) the Dirac region ($n \lesssim 7 \times 10^{10}$ cm^{-2}) and (b) electron region ($n \simeq 10^{12}$ cm^{-2}); (c) Phase-breaking rate $\tau_\phi^{-1} = D/L_\phi^2$ as a function of T for different n. Inset to (a) illustrates the saturation of L_ϕ at low T due to the sample size. Inset to (b) shows the scattering process behind the length L_i. Sample F2: (d) Temperature dependence of the characteristic lengths in the electron region ($n \simeq 10^{12}$ cm^{-2}).

region. Sample F2 is about 3 times longer, and one can see that $L_\phi^{\rm sat}$ is larger in the longer sample $F2$. (In sample B, $L_\phi^{\rm sat}$ has also been found to be larger than in sample D.) This clearly implies that the reason for the saturation is a limitation imposed by the sample size, and not by scattering from a small, uncontrolled number of magnetic impurities [3].

In the Dirac region $L_\phi^{\rm sat}$ has been found to have a smaller value than at larger carrier densities. (It is interesting to note that the narrow sample, B, shows the biggest decrease of $L_\phi^{\rm sat}$ in the Dirac region, while the square sample, D, the smallest.) This decrease can be related to the inhomogeneity of the sample at low carrier densities. It can result in formation of electron-hole puddles, so that at $V_g = 0$ there are equal densities of electrons and holes and not zero density of each type of carrier. Inhomogeneity can modify the geometry of conducting paths and decrease the effective dimensions of the sample, resulting in a smaller value of $L_\phi^{\rm sat}$.

The temperature dependence of L_ϕ contains information about the inelastic mechanism responsible for the dephasing of charge carriers. There are suggestions that electron-electron (e-e) interaction, the main mechanism of dephasing at low T, is different in graphene compared with other systems [15]. To examine this we have analyzed the T-dependence of the dephasing rates found from analysis of the WL. Figure 3(c) shows the phase-breaking rate in different density regions of sample D. (To find τ_ϕ^{-1} we use the relation $L_\phi = (D\tau_\phi)^{1/2}$, where the diffusion coefficient $D = v_F l/2$ is determined from the mean free path $l = h/2e^2 k_F \rho$. For the Dirac region, where the puddles can be formed, the value of the Fermi wave number k_F (inside the puddle) is simply estimated at the boundary of the region where the MC is studied, $|V_g| = 1$ V, Fig. 1). Our results show that electron dephasing rate obeys the usual, linear T-dependence for e-e scattering in the "dirty limit", $T\tau_p < 1$ [1]: $\tau_\varphi^{-1} = \beta k_B T \ln g/\hbar g$, where $g = \sigma h/e^2$. (In our samples the parameter $T\tau_p$ varies from 0.002 to 0.4 in the studied temperature range 0.25–25 K.) The empirical coefficient β is found to be between 1 and 2 in all studied regions and all samples. Therefore, we can conclude that while electron interference in graphene is significantly different from other systems, e-e interaction does not show unconventional behavior.

In addition to the analysis of the WL, we have also analyzed conductance fluctuations as a function of B and V_g using standard relations in terms of L_ϕ [2]. This analysis has given values of L_ϕ close to those found from the analysis of WL [13].

Now let us discuss the behavior of the elastic, intervalley length L_i which we have verified to be essentially T independent in all samples. In samples D, F1, and F2 the found L_i is comparable to the width of the samples (approximately half the width). This means that, indeed, the sample edges make significant contributions to intervalley scattering. This is consistent with the fact that the narrowest sample B has shown the smallest value of L_i. However, the value of L_i for sample B is about 3 times smaller than the sample width. This can be due to the presence of rapid ridges of height $\sim$1.5 nm observed in this sample by AFM, Fig. 4(a). They are separated by a distance smaller than the sample width and can be another source of intervalley scattering. This suggests that the intervalley scattering is controlled not only by the edges but also by the defects in the inner part of the sample.

We have found that the intravalley scattering length L_* is much smaller than the intervalley length L_i, Fig. 3, and approaches the mean free path. There are several possible mechanisms that can be responsible for the observed large intravalley scattering rate and resulting strong suppression of WL in one valley [13]. Scattering by *atomically sharp defects* cannot explain this: such scattering is also a source of strong intervalley scattering, so that L_i and L_* would be comparable if this mechanism was dominant. The smaller value of L_* in experiment must therefore be due to an additional scattering rate which affects L_* but not L_i: from *warping* [8], or from the defects of the crystal struc-

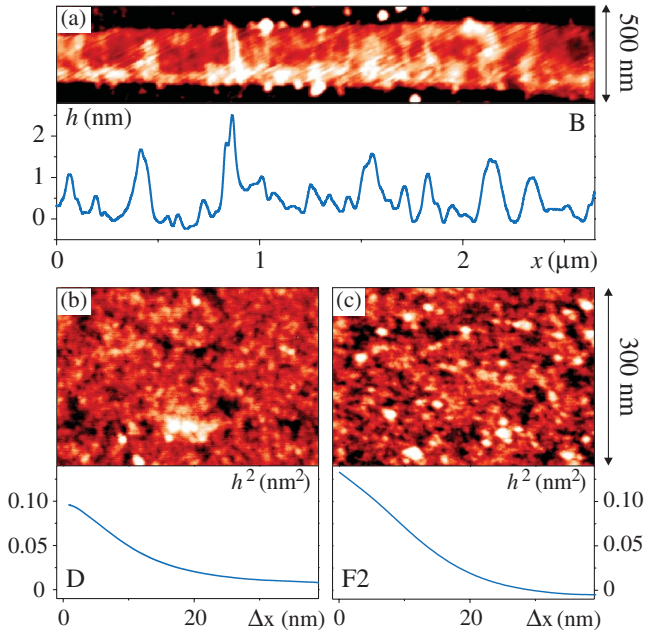

FIG. 4 (color). Atomic force microscope images of graphene surfaces. Below the image of sample B (a) is the surface profile averaged over the width of the sample. Below the images of the topography of samples D (b) and F2 (c) are the corresponding autocorrelation functions of the surface roughness.

ture that are large on the atomic scale [5,10]. Estimation of the expected τ_w^{-1} using theory [8] gives a value of $\tau_w^{-1} \leq 0.3\ \mathrm{ps}^{-1}$ which is much smaller than the experimental $\tau_*^{-1} \sim 10\ \mathrm{ps}^{-1}$. Therefore, the reason for small L_* could lie in the defects of the crystal structure of graphene flakes: *ripples* and *dislocations*. (The strain in the lattice induced by such defects acts as a source of effective magnetic field that can destroy WL.) As the dislocation core is also a source of intervalley scattering, their separation can be estimated from the known value of L_i. This value is much larger than the dislocation separation $\xi \sim 50$ nm required to explain the small value of L_*. (This value of ξ is obtained using the relation $\tau_s^{-1} = v_F/k_F\xi^2$ [10].) The effect of ripples on the graphene surface is also negligible in our samples, if we use the estimation of this effect from [5]. The roughness of our samples found from AFM measurements, Figs. 4(b) and 4(c), is of height $h \simeq 0.3$ nm and lateral size $d \simeq 10$ nm (in agreement with [16]), which gives for a typical $L_\phi \approx 1\ \mu$m an effective magnetic field $B_{\mathrm{eff}} \sim 1$ mT. This is a small correction to the real fields used in experiment, Fig. 2. There is one more mechanism that can introduce an asymmetry in the crystal structure and hence break the chirality of carriers: a potential gradient coming from charged impurities in the substrate. Our estimation of its effect using the approach of [10] has also given a negligible result [13]. Therefore, the obtained values of the scattering rate τ_*^{-1} are much higher than those predicted by existing models, and more detailed theories of the mechanisms of intravalley suppression of WL in graphene are required.

In summary, we have shown that the weak localization correction in graphene exists at all studied carrier densities, including the Dirac region. Its manifestation is determined by the interplay of inelastic and elastic scattering mechanisms, which makes WL a sensitive tool to detect the defects responsible for intervalley scattering and chirality breaking. We show that, in spite of a strong intravalley suppression of WL, the quantum interference correction to the conductivity is clearly seen due to significant intervalley scattering. Total suppression of WL is only possible in experiments where intervalley scattering is negligible, i.e., in very large samples without sharp defects in the bulk.

We gratefully acknowledge stimulating discussions with E. McCann, V. V. Cheianov, F. Guinea, and V. I. Fal'ko, and thank B. Wilkinson for assistance at an early stage of the experiments. We also thank EPSRC for funding.

[1] B. L. Altshuler, D. Khmelnitzkii, A. I. Larkin, and P. A. Lee, Phys. Rev. B **22**, 5142 (1980); G. Bergman, Phys. Rep. **107**, 1 (1984).
[2] C. W. J. Beenakker and H. Van Houten, in *Solid State Physics*, edited by H. Ehrenreich and D. Turnbull (Academic, San Diego, 1991), Vol. 44, p. 1.
[3] F. Pierre, A. B. Gougam, A. Anthore, H. Pothier, D. Esteve, and N. O. Birge, Phys. Rev. B **68**, 085413 (2003).
[4] K. S. Novoselov *et al.*, Science **306**, 666 (2004).
[5] S. V. Morozov *et al.*, Phys. Rev. Lett. **97**, 016801 (2006).
[6] H. B. Heersche *et al.*, Nature (London) **446**, 56 (2007).
[7] X. Wu, X. Li, Z. Song, C. Berger, and W. A. de Heer, Phys. Rev. Lett. **98**, 136801 (2007).
[8] E. McCann *et al.*, Phys. Rev. Lett. **97**, 146805 (2006).
[9] H. Suzuura and T. Ando, Phys. Rev. Lett. **89**, 266603 (2002).
[10] A. F. Morpurgo and F. Guinea, Phys. Rev. Lett. **97**, 196804 (2006).
[11] T. Ando, T. Nakanishi, and R. Saito, J. Phys. Soc. Jpn. **67**, 2857 (1998).
[12] A. K. Geim and K. S. Novoselov, Nat. Mater. **6**, 183 (2007).
[13] See EPAPS Document No. E-PRLTAO-100-052805 for supplementary material. For more information on EPAPS, see http://www.aip.org/pubservs/epaps.html.
[14] R. V. Gorbachev, F. V. Tikhonenko, A. S. Mayorov, D. W. Horsell, and A. K. Savchenko, Phys. Rev. Lett. **98**, 176805 (2007).
[15] J. Gonzalez, F. Guinea, and M. A. H. Vozmediano, Phys. Rev. Lett. **77**, 3589 (1996); J. Gonzalez, F. Guinea, and M. A. H. Vozmediano, Phys. Rev. B **59**, R2474 (1999); S. Das Sarma, E. H. Hwang, and W.-K. Tse, Phys. Rev. B **75**, 121406(R) (2007); M. Polini, R. Asgari, Y. Barlas, T. Pereg-Barnea, and A. H. MacDonald, Solid State Commun. **143**, 58 (2007).
[16] M. Ishigami, J. H. Chen, W. G. Cullen, M. S. Fuhrer, and E. D. Williams, Nano Lett. **7**, 1643 (2007).